Electrostatic and Conformational Effects on the Electronic Structures of Distortional Isomers of a Mixed-Valence Binuclear Cu Complex

Stefan Franzen,*,† Vincent M. Miskowski,‡ Andrew P. Shreve,‡ Stacie E. Wallace-Williams,‡ William H. Woodruff,‡ Mark R. Ondrias,§ Mary E. Barr,|| Laura Moore,⊥ and Steven G. Boxer⊥

Department of Chemistry, North Carolina State University, Raleigh, North Carolina 27695, Bioscience and Nuclear Materials and Technology Divisions, Los Alamos National Laboratory, Los Alamos, New Mexico 87545, Department of Chemistry, University of New Mexico, Albuquerque, New Mexico 87131, and Department of Chemistry, Stanford University, Stanford, California 94305

Received May 11, 2001

The electronic structure of the binuclear copper complex $[Cu_2(L)]^{3+}$ [L = $N(CH_2CH_2N(H)CH_2CH_2N(H)CH_2CH_2)_3N$] has been investigated by resonance Raman and electroabsorption spectroscopy. Crystallographic Cu_2 distances of 2.364(1) and 2.415(1) Å determined for the nitrate and acetate salts, respectively, are consistent with a substantial metal−metal interaction. The Cu−Cu bonding interaction in the binuclear complex is modulated both in the solid state and in solution by the ligand environment through coupling to ligand torsional modes that are, in turn, stabilized by hydrogen bonding. Electroabsorption data on the three major visible and near-infrared electronic transitions of Cu_2L, λ_{max} (ϵ_{max}) = 1000 nm (∼1200 M^{-1} cm^{-1}), 748 nm (5600 M^{-1} cm^{-1}), and 622 nm (3350 M^{-1} cm^{-1}), reveal a difference dipole moment between the ground and excited states ($\Delta\mu_A$) because of symmetry breaking. The difference polarizability for all three of the transitions is negative, indicating that the ground state is more polarizable than the excited state. A general model to explain this behavior in terms of the proximity of accessible transitions involving copper d electrons is proposed to explain the larger polarizability of the ground state. Raman excitation profiles (REPs) provide evidence for multiple conformational states of $[Cu_2(L)]^{3+}$. Separate REPs were obtained for each of the components of the two major Raman bands for ν_1 (a Cu−Cu stretching mode) and ν_2 (a Cu−Cu−N_{eq} bending mode). The Raman data along with quantum chemical ZINDO/S CI calculations provide evidence for isomeric forms of Cu_2L with strong coupling between the conformation of L and the Cu−Cu bond length.

Introduction

The electronic structure of binuclear copper complexes provides a unique combination of mixed valency and flexible coordination that has important functional consequences in biology.[1−7] The Cu_A center of cytochrome *c* oxidase and nitrite reductase consists of a mixed-valence Cu_2 site in their respective resting states.[1−9] There is an increasing consensus that the weak Cu−Cu bonding in these proteins allows the protein to exert conformational and electrostatic control over electron transfer at the Cu_A site.[6,9,10] Numerous model compounds have been prepared that show similar properties of Cu(I)/Cu(II) mixed valency and conformational flexibility.[9,11−15]

We have shown in a previous study that the Cu−Cu bonding interaction in a model binuclear complex is modulated both in solution and in the solid state by the ligand environment through coupling to ligand torsional modes that are, in turn, stabilized

† North Carolina State University.
‡ Bioscience Division, Los Alamos National Laboratory.
|| Nuclear Materials and Technology Division, Los Alamos National Laboratory.
§ University of New Mexico.
⊥ Stanford University.

(1) Andrew, C. R.; Lappalainen, P.; Saraste, M.; Hay, M. T.; Lu, Y.; Dennison, C.; Canters, G. W.; Fee, J. A.; Slutter, C. E.; Nakamura, N.; Sanders-Loehr, J. *J. Am. Chem. Soc.* **1995**, *117*, 10759−10760.
(2) Andrew, C. R.; Fracziewicz, R.; Czernuszewicz, R. S.; Lappalainen, P.; Saraste, M.; Sanders-Loehr, J. *J. Am. Chem. Soc.* **1996**, *118*, 10436−10445.
(3) Cole, J. L.; Clark, P. A.; Solomon, E. I. *J. Am. Chem. Soc.* **1990**, *112*, 9534−9548.
(4) Meyer, T. E.; Marchesini, A.; Cusanovich, M. A.; Tollin, G. *Biochemistry* **1991**, *30*, 4619−4623.
(5) Wallace-Williams, S. E.; James, C. A.; DeVries, S.; Saraste, M.; Lappalainen, P.; van der Oost, J.; Fabian, M.; Palmer, G.; Woodruff, W. H. *J. Am. Chem. Soc.* **1996**, *118*, 3986−3987.
(6) Randall, D. W.; Gamelin, D. R.; LaCroix, L. B.; Solomon, E. I. *J. Inorg. Biochem.* **2000**, *5*, 16−29.
(7) Farrar, J. A.; Neese, F.; Lappalainen, P.; Kroneck, P. M. H.; Saraste, M.; Zumft, W. G.; Thomson, A. J. *J. Am. Chem. Soc.* **1996**, *118*, 11501−11514.
(8) Blackburn, N. J.; de Vries, S.; Barr, M. E.; Houser, R. P.; Tolman, W. B.; Sanders, D.; Fee, J. A. *J. Am. Chem. Soc.* **1997**, *119*, 6135−6143.
(9) Kroneck, P. M. H.; Antholine, W. E.; Kastrau, D. H. W.; Buse, G.; Steffens, G. C. M.; Zumft, W. G. *FEBS Lett.* **1990**, *268*, 274−276.
(10) Williams, K. R.; Gamelin, D. R.; LaCroix, L. B.; Houser, R. P.; Tolman, W. B.; Mulder, T. C.; deVries, S.; Hedman, B.; Hodgson, K. O.; Solomon, E. I. *J. Am. Chem. Soc.* **1997**, *119*, 613−614.
(11) Nelson, J.; McKee, V.; Morgan, G. *Prog. Inorg. Chem.* **1998**, *47*, 167−316.
(12) LeCloux, D. D.; Davydov, R.; Lippard, S. J. *Inorg. Chem.* **1998**, *37*, 6814−6826.
(13) Hay, M. T.; Ang, M. C.; Gamelin, D. R.; Solomon, E. I.; Antholine, W. E.; Ralle, M.; Blackburn, N. J.; Massey, P. D.; Wang, X. T.; Kwon, A. H.; Lu, Y. *Inorg. Chem.* **1998**, *37*, 191−198.
(14) Barr, M. E.; Smith, P. H.; Antholine, W. E.; Spencer, B. *J. Chem. Soc., Chem. Commun.* **1993**, 1649−1652.
(15) Al-Obaidi, A.; Baranovie, G.; Coyle, J.; Coates, C.; McGarvey, J. J..; McKee, V.; Nelson, J. *Inorg. Chem.* **1998**, *37*, 3567−3574.

10.1021/ic010494g CCC: $20.00
Published on Web 11/03/2001

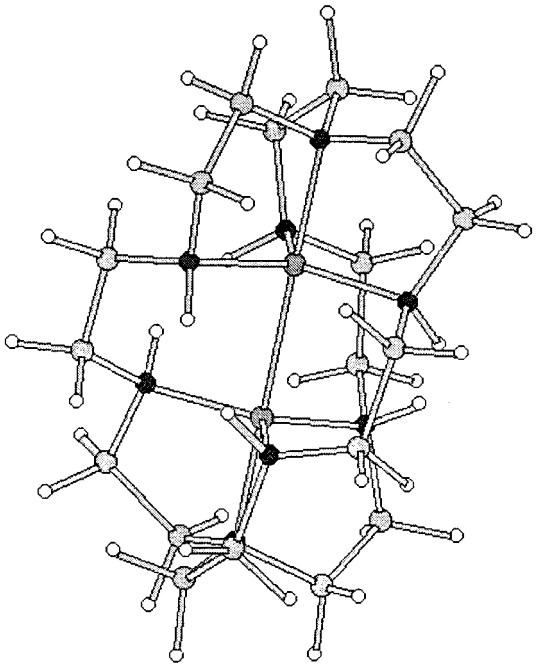

Figure 1. Representation of the structure of Cu_2L from the coordinates for the nitrate salt obtained from X-ray crystallography.[13]

by hydrogen bonding.[16] The complex $[Cu_2(L)]^{3+}$ [L = $N(CH_2CH_2N(H)CH_2CH_2N(H)CH_2CH_2)_3N$] contains a $Cu^{1.5}-Cu^{1.5}$ unit stabilized by encapsulation in the octaaza-cryptand ligand L and has been crystallized with both acetate and nitrate counterions (Figure 1).[14] The complex is thermally stable and is soluble in a range of solvents from benzene to water, depending on the identity of the counterion. The optical absorption and MCD spectra are quite similar to those of the Cu_A center of resting cytochrome oxidase,[17] and EPR establishes a completely delocalized ($Cu^{1.5}$) valence state under a variety of conditions. Crystallographic Cu_2 distances of 2.364(1) and 2.415(1) Å determined for the nitrate and acetate salts, respectively, are consistent with a substantial metal−metal interaction.[14]

Preliminary data[16] revealed that the ν(Cu−Cu) stretching Raman band (ν_1) and the δ(Cu−Cu−N_{eq}) bend (ν_2) appear as single resonance Raman bands in each of the two crystalline forms of Cu_2L, with the energies of the nitrate salt being ∼2−3 cm^{-1} higher in frequency as expected for the shorter Cu−Cu bond. In aqueous solutions, however, each band consists of three components whose relative populations are sensitive to temperature, solvent, and excitation wavelength, as shown in Figure 2. Comparison of $^{63}Cu/^{65}Cu$ isotope data[16] and a normal-mode analysis suggests that these components are not different normal modes but rather that they are the slightly shifted frequencies of multiple conformers of Cu_2L in solution (see the Supporting Information and ref 15). This intriguing behavior has prompted us to investigate more fully the ties between the physical structure of this complex and its electronic properties.

To better understand the nature of the electronic transitions in solution, we have obtained electroabsorption data on the three major visible and near-infrared electronic transitions of Cu_2L. Electroabsorption spectroscopy has been used to determine the charge-transfer character of mixed-valent inorganic complexes. In an early report that studied a metal-to-ligand charge-transfer (MLCT) transition of $Ru(bipy)_3^{2+}$, a large change in the dipole moment was noted despite the presence of the idealized D_3 symmetry of the complex in the ground state.[18] Symmetry breaking may arise because of interactions with the counterions or the surrounding solvent, which may act in conjunction with vibronic coupling mechanisms. In either case, the result appears to be the localization of the MLCT state, with a corresponding change in dipole upon excitation, in a complex whose idealized point group cannot support a permanent dipole. The idealized symmetry of Cu_2L is also D_3, and thus, the difference dipole moment between the ground and excited states ($\Delta\mu_A$) should be zero if the symmetry of the metal complex is considered in isolation. However, as shown in this paper, the measured $\Delta\mu_A$ is not zero for any of the electronic absorption transitions. The measured angle dependence of the electroabsorption effect permits a determination of the projection of $\Delta\mu_A$ on the transition moments of the respective electronic transitions. This measurement provides evidence that symmetry breaking occurs because of the electrostatic field of the counterions in solutions of Cu_2L, as was found for the $Ru(bipy)_3^{2+}$ complex. The breaking of molecular symmetry by ancillary species may play a key role in electroabsorption spectra of centrosymmetric inorganic complexes.

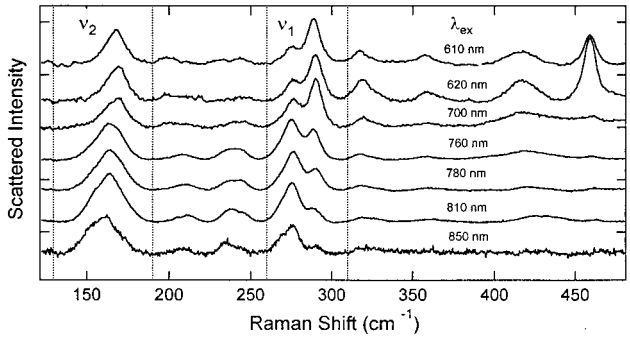

Figure 2. Resonance Raman spectra of $Cu_2L(NO_3)_3$ in H_2O. The Cu−Cu stretching vibration ν_1 and the Cu−Cu−N_{eq} bending mode ν_2 both show a pronounced change in band composition as a function of the excitation wavelength.

The present work explores both the conformational and electrostatic effects of the environment on the properties of Cu−Cu bonded systems by a combination of resonance Raman and electroabsorption spectroscopy. Herein, we examine the correlation between the frequency maximum of distinct relative Raman excitation profiles (REPs) for each of the components of ν_1 and ν_2 and the component Raman band frequencies. The analyses of the electronic structures using electronic structure calculations together with the depolarization ratios of $\approx^1/_3$ for ν_1 and ν_2 with a 760 nm excitation indicate that the vibrational modes are totally symmetric (Franck−Condon) modes and that the electronic absorption is polarized along the Cu−Cu axis (molecular *z* axis).[16] These considerations, along with quantum chemical ZINDO/S CI calculations, strengthen the hypothesis that the REPs reflect specific isomeric forms of Cu_2L with strong coupling between the conformation of L and the Cu−Cu bond length.

Experimental Section

Room-temperature resonance Raman measurements were performed on solutions of Cu_2L. Isotopic shifts were measured by repetitively placing the natural abundance and isotopically labeled samples in the laser beam for alternating 2 min data acquisition periods. A typical

(16) Miskowski, V. M.; Franzen, S.; Shreve, A. P.; Wallace-Williams, S. E.; Barr, M.; Woodruff, W. H. *Inorg. Chem.* **1999**, *38*, 2546−2547.
(17) Farrar, J. A.; McKee, V.; Al-Obaidi, A. H. R.; McGarvey, J. J.; Nelson, J.; Thomson, A. J. *Inorg. Chem.* **1995**, *34*, 1302−1303.
(18) Oh, D. H.; Boxer, S. G. *J. Am. Chem. Soc.* **1989**, *111*, 1130−1131.

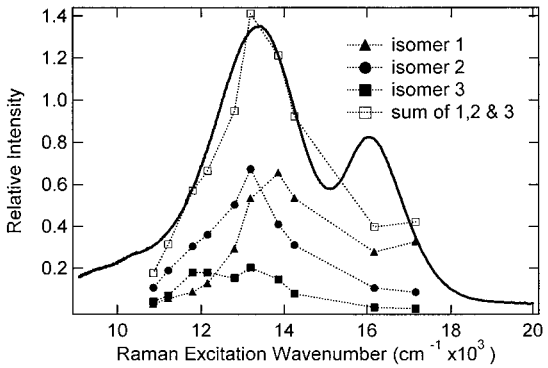

Figure 3. Relative resonance Raman excitation profiles (REPs) of ν_1 for each of three isomeric forms of $Cu_2L(NO_3)_3$. The intensities were determined relative to an ethylene glycol internal standard. The sum of the intensity for the three isomeric forms is also plotted in comparison to the room-temperature absorption spectrum.

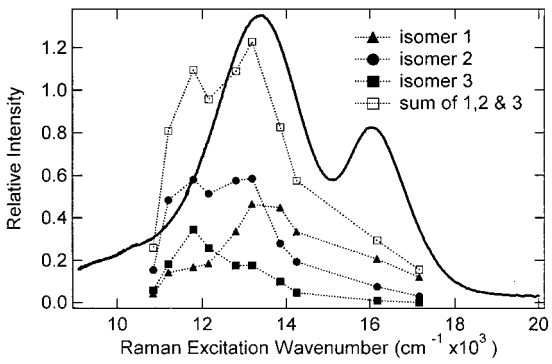

Figure 4. Relative resonance Raman excitation profiles (REPs) of ν_2 for each of three isomeric forms of $Cu_2L(NO_3)_3$. The intensities were determined relative to an ethylene glycol internal standard. The sum of the intensity for the three isomeric forms is also plotted in comparison to the room-temperature absorption spectrum.

data set consisted of 10 repetitions for a total of 20 min of data acquisition time. Room-temperature solution samples were prepared either in an aqueous solution or in a 50% ethylene glycol aqueous solution. The ethylene glycol peaks at 346 and 481 cm^{-1} served as an internal standard for the determination of relative resonance Raman profiles. Solutions were studied at several concentrations in the range from 2 to 10 mM to ascertain experimentally that inner-filter effects were negligible at the concentration where the intensities of ethylene glycol bands were compared. Corrections for detector response were not applied. Solid-state resonance Raman spectra were obtained by diluting the crystalline sample in KBr powder to obtain a concentration similar to that used for the solution measurements. Raman spectra at 40 K were obtained by placing the sample on the gold-plated coldfinger of a Displex closed-cycle helium refrigerator. Near-infrared Raman spectra were obtained with a SpectraPhysics argon ion laser-pumped SpectraPhysics 3090 Ti:sapphire laser operating between 700 and 920 nm. Typical slit widths were 100 μm, although larger slit widths were used at excitation wavelengths greater than 850 nm. The scattered Raman light was collected using lenses, dispersed using a SPEX 1807 triple monochromator/spectrograph, and then detected using a liquid-nitrogen-cooled Princeton Instruments CCD camera. A separate Raman spectrometer was used for visible resonance Raman experiments. A Coherent 590 dye laser (Rhodamine 6-G dye) pumped by the visible lines of a Coherent Innova 400 argon ion laser provided output between 560 and 620 nm. Typical laser powers were 50 mW. Argon ion lines were used at 514.5, 501, and 488 nm. A Coherent Antares 76S provided quasi continuous wave output at 532 nm. Scattered light was collected by a f/1 5 cm focal length lens and focused on the slit of a SPEX 1807. Slit widths were set to 50 μm to provide a 2.5 cm^{-1} resolution on a Photometrics CCD camera.

Electroabsorption measurements were conducted on a sample of $Cu_2L(NO_3)_3$ placed between two microscope slides coated with indium tin oxide. The spacer thickness was 25 μm. The sample was placed in a liquid-nitrogen Dewar with strain-free quartz windows. The electroabsorption apparatus and analysis have been described elsewhere.[19]

Results

The absorption spectra are crucial to understanding both the resonance Raman and the electroabsorption data. The electronic absorption bands in aqueous solution are λ_{max} (ϵ_{max}) = 1000 nm (10 000 cm^{-1}, ~1200 M^{-1} cm^{-1}), 748 nm (13 400 cm^{-1}, 5600 M^{-1} cm^{-1}), and 622 nm (16 100 cm^{-1}, 3350 M^{-1} cm^{-1}), labeled I−III, respectively. The room-temperature absorption spectrum of $Cu_2L(NO_3)_3$ is shown with resonance Raman excitation profiles for modes ν_1 and ν_2 in Figures 3 and 4, respectively. While band I is ill-defined, bands II and III appear to be simple, although broad, absorption bands. The absorption bands at 77 K are better resolved, as seen in the electroabsorption data in Figure 5; however, at both temperatures, band fitting indicates that there may be more than one absorption band underlying each of the transitions.[16]

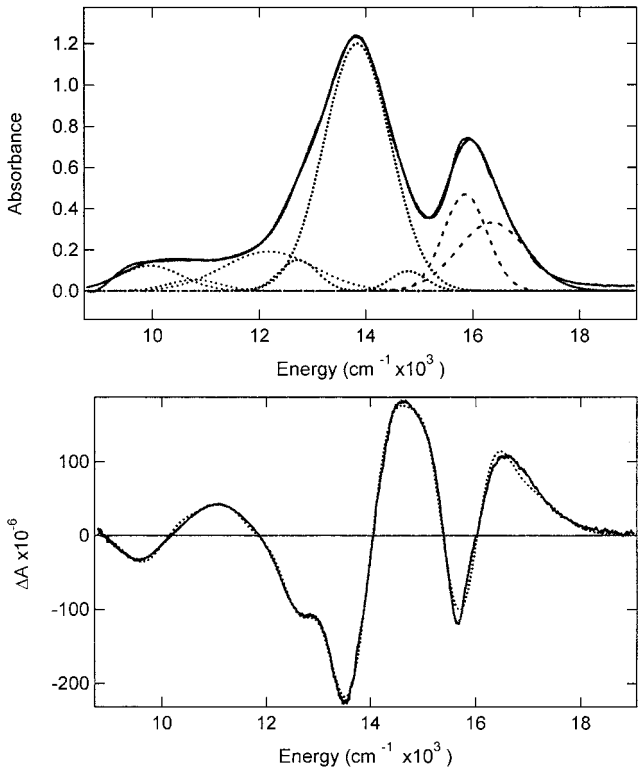

Figure 5. Electroabsorption data for $Cu_2L(NO_3)_3$ obtained at 77 K in a glycerol/buffer glass. (a) The upper panel shows the absorption spectra for bands I−III. The dashed lines represent the individual Gaussians from the fit to those bands given in Table 4 of the Supporting Information. (b) The lower panel shows the change in absorbance in an applied electric field (—) and the fit to the data using derivatives according to the Liptay formalism[24] (···). The electric field strength is 0.77 MV cm^{-1}, and the experimental angle between the electric vector of the light and the applied field is $\chi = 52°$.

Resonance Raman excitation profiles of the major bands ν_1 and ν_2 were obtained in the range of 580−920 nm by laser excitation of $Cu_2L(NO_3)_3$ in aqueous solution at room temperature. There are a number of higher frequency bands observed in resonance with band III (λ_{max} = 622 nm) that we assign to equatorial ligand deformation modes (see the Supporting

(19) Bublitz, G. U.; Boxer, S. G. *Annu. Rev. Phys. Chem.* **1997**, *48*, 213−242.

Information). The REP is reported only for the most intense features observed for excitation in resonance with band II (λ_{max} = 748 nm) that appear as two strong resonantly enhanced modes in the 140−170 cm^{-1} (ν_2) and 265−290 cm^{-1} (ν_1) regions. These bands have been previously assigned on the basis of the $^{63}Cu/^{65}Cu$ isotope effect and a valence force field analysis[16] (also see the Supporting Information). [The partitioning of $\nu(Cu_2)$ obtained from this calculation is in general agreement with the results of an independent normal-mode determination recently performed by McGarvey and co-workers. However, the details of the two calculations differ in that those reported in ref 15 assign independent normal modes to the multiple-band features that are here assigned as features of multiple conformational isomers that exist in solution.] Raman band ν_2 arises from $\delta(Cu-Cu-N_{eq})$ bending (77% of the potential energy distribution (PED)), and most of the remaining contribution to the PED comes from the Cu−Cu stretch. Raman band ν_1 is mostly a Cu−Cu stretching vibration (64% of the PED), although it does have a minor contribution from $\delta(Cu-Cu-N_{eq})$ as well. These are A_{1g} bands that are Franck−Condon-active for the $\sigma \rightarrow \sigma^*$ transition. The weak band at ≈210 cm^{-1} may be an A_{2u} band that is vibronically active (see the Supporting Information). The band observed at ≈316 cm^{-1} is an overtone of ν_2. There is an apparent structure to ν_1, and the asymmetric shape of ν_2 also implies structure. Both ν_1 and ν_2 were fitted to three Gaussian components at each excitation wavelength, as presented previously (see the Supporting Information).[16] REPs were calculated for each of the components of ν_1 and ν_2 at various excitation wavelengths on the basis of their relative ratios as determined from the Gaussian fits. These individual REPs are shown in Figures 3 and 4, respectively, along with the room-temperature absorption spectrum of $Cu_2L(NO_3)_3$.

The justification for treating the components of ν_1 and ν_2 as contributions from discrete conformers of $Cu_2L(NO_3)_3$ rather than as distinct normal modes of vibration can be found in the previously reported isotope data[16] and in the correlation between the REPs and component Raman band frequency that we present here. In $^{63}Cu/^{65}Cu$ isotopically labeled Cu_2L, ν_1 and ν_2 appear as multiple bands whose components shift by 2.5 and 0.7 cm^{-1}, respectively. A fit of a valence force field to these data is consistent only with multiple isomers of the Cu dimer cryptand Cu_2L rather than with distinct Raman-active modes as an assignment for the components seen in Figure 2 (see the Supporting Information). The relative Raman intensity of the bands in the REP and the error estimated from the fits are given in Table 1. The presence of multiple REPs with slightly different mode frequencies suggests a correlation between the force constant of the ν(Cu−Cu) stretching internal coordinate (as reflected in the frequency of the vibrational modes ν_1 and ν_2) and the energy of the electronic transition. This correlation is explored in ZINDO/S CI presented in this paper. The REPs shown in Figures 3 and 4 indicate that the observed electronic absorption bands may be comprised of overlapping bands from three conformational isomers, each with a slightly different absorption spectrum.

Fitting of the room-temperature data alone does not give a clear indication of the proper composition of the spectra. It is more instructive to examine the structure in the absorption bands of solutions frozen in liquid nitrogen at 77 K. Under these conditions, bands II and III narrow sufficiently to allow enhanced resolution of the near-infrared band I, and bands II and III now exhibit an asymmetry of structure that is hidden in the room-temperature absorption spectrum. The fit to the absorption spectrum is shown in Figure 5 for data obtained at 77 K.

Table 1. Relative Raman Excitation Profiles (REPs) for ν_1 and ν_2

A. REPs for ν_1

λ_{ex} (nm)	**1** (290 cm^{-1})	**2** (277 cm^{-1})	**3** (270 cm^{-1})
583	0.32(2)	0.086(6)	0.0073(7)
618.2	0.27(3)	0.11(1)	0.013(5)
701.95	0.53(4)	0.31(1)	0.078(5)
721.6	0.65(5)	0.41(2)	0.15(2)
758.2	0.53(3)	0.67(3)	0.20(2)
780.76	0.29(2)	0.50(3)	0.15(1)
822.9	0.12(8)	0.36(2)	0.18(3)
848.2	0.08(2)	0.30(3)	0.18(4)
892.5	0.05(2)	0.18(5)	0.07(3)
921.7	0.03(1)	0.10(4)	0.04(2)

B. REPs for ν_2

λ_{ex} (nm)	**1** (174 cm^{-1})	**2** (164 cm^{-1})	**3** (153 cm^{-1})
583	0.12(2)	0.032(4)	0.0027(3)
618.2	0.20(2)	0.076(7)	0.011(2)
701.95	0.33(3)	0.19(3)	0.049(5)
721.6	0.44(5)	0.27(3)	0.10(2)
758.2	0.46(4)	0.58(5)	0.17(2)
780.76	0.33(2)	0.57(6)	0.17(1)
822.9	0.18(2)	0.51(4)	0.25(2)
848.2	0.16(3)	0.58(6)	0.34(4)
892.5	0.14(4)	0.48(4)	0.18(3)
921.7	0.04(1)	0.15(6)	0.06(2)

Both the broad absorption band I and the intense feature at band II require three Gaussians to obtain a satisfactory fit, while band III can be fit with only two Gaussians. The fitting parameters for all three of the electronic absorption bands at 77 K are given in the Supporting Information. Although it is clear that there is some structure associated with each of the bands, the unambiguous determination of the components is still obscured by overlapping bands. This problem is particularly noticeable in the region between bands II and III. For example, the broadest band at the highest wavenumber value inside the envelope of band II could be narrower if part of the intensity were due to the narrow band inside the envelope of band III. These types of issues complicate the quantitative resolution of the components using only the absorption spectrum. However, as shown in Figure 5, the peculiar shape of the absorption band obtained at 77 K can only be fit by three components in a manner consistent with the analysis of the resonance Raman spectroscopy.

Because of the lack of apparent structure in the room-temperature absorption spectrum, it is important to consider the implications of Raman data obtained at cryogenic temperatures in comparison with the absorption spectrum in Figure 5 obtained at 77 K. The Raman spectra at 40 K are qualitatively similar to those at room temperature (see the Supporting Information). This is important because it indicates that the exchange between the isomeric forms of Cu_2L in solution is slow enough that it is frozen-in at cryogenic temperatures. Moreover, the existence of multiple bands in both resonance Raman and absorption spectra obtained at cryogenic temperatures indicates the possibility that there is a relationship between the frequency of the Raman band and the absorption maximum, as implied by the room-temperature REPs shown in Figures 3 and 4.

Electroabsorption data shown in Figure 5 were obtained at 77 K in a frozen glycerol/buffer glass. The electroabsorption data could be well fit by simultaneously fitting the absorption and electroabsorption data to a model that consisted of three Gaussians per band (absorption) and the zero, first, and second

Table 2. Difference Dipole Moments, Polarizabilities, and Angles Obtained from Fits of the Electroabsorption Data as a Function of Experimental Angle χ

	band I (1000 nm)	band II (750 nm)	band III (620 nm)
$\Delta\mu_A$ (D)	2.3 ± 0.4	1.2 ± 0.3	0.9 ± 0.2
ζ_A	45 ± 4	62 ± 5	43 ± 5
$\Delta\alpha$ (Å^3)	-67 ± 8	-41 ± 6	-32 ± 5
Tr($\Delta\alpha$) (Å^3)	-30 ± 4	-19 ± 4	-10 ± 3

derivatives of those Gaussians (electroabsorption) for bands I and II and of a two-Gaussian model for band III. The band structure is identical to that shown in Figure 5. [The fit to the data in the electroabsorption spectrum is a simultaneous fit to both the absorption spectrum and the electroabsorption spectrum. By using three Gaussians for bands I and II and two Gaussians for band III, this is an eight-Gaussian fit. The model does differ from that obtained from the fit of the absorption spectrum alone, as shown by the comparison of the parameters given in the Supporting Information.] The data obtained at various experimental angles χ between the applied electric field and the electric vector of the light were fit. The second-derivative components of these fits were used to extract the difference dipole moment for absorption ($\Delta\mu_A$) and the angle (ζ_A) between the transition moment and $\Delta\mu_A$. The first-derivative components of the fits were used to extract the difference polarizability ($\Delta\alpha$) and the magnitude of the trace of the difference polarizability. These values are given in Table 2. Surprisingly, the difference polarizability for all three of the transitions is negative, indicating that the ground state is more polarizable than the excited state. This conclusion can also be reached by inspection of Figure 5, because the electroabsorption data show an absorption band shift (first derivative) to higher energy for the three absorption bands. The angle ζ_A in band II (750 nm band) is greater than 54.7° (the magic angle). This too is unusual because it indicates that the direction of charge displacement ($\Delta\mu_A$) in the excited state is not aligned with the transition moment. This is not the case for bands I and III, where ζ_A is ca. 45° but still less than the magic angle. Comparisons of the absorption spectrum of $Cu_2L(CH_3CO_2)_3$ in acetonitrile/water indicate that solvatochromic shifts occur for all three of the bands. Band I appears broader in an acetonitrile solution than in an aqueous solution (see the Supporting Information). Bands II and III have nearly the same bandwidth but are substantially shifted to higher energies. The solvent effects follow the same trend as the difference dipole moments in the electroabsorption spectra. For example, when acetonitrile and water are compared, the band shifts are very large (i.e., >1000 cm^{-1}) for band I, 610 cm^{-1} for band II, and 410 cm^{-1} for band III.

ZINDO/S CI calculations of a model of Cu_2L were performed to determine the electronic structure for comparison with both the Raman and electroabsorption data (see the Supporting Information). The calculations assigned the electronic transitions as $\delta \rightarrow \sigma^*$ (1000 nm), $\sigma \rightarrow \sigma^*$ (750 nm), and $\delta^* \rightarrow \sigma^*$ (620 nm). [Extended Huckel theory (EHT) calculations performed in collaboration with Dr. M. Whangbo yielded a slightly different picture. The EHT results indicated that the electronic transitions are assigned as $\delta,\delta^* \rightarrow \sigma^*$ (1000 nm), $\sigma \rightarrow \sigma^*$ (750 nm), and $\pi,\pi^* \rightarrow \sigma^*$ (620 nm). The two calculations are consistent in that $\sigma \rightarrow \sigma^*$ is the intermediate energy transition and that it has the largest oscillator strength.] The assignment of the 750 nm band as $\sigma \rightarrow \sigma^*$ can be reconciled with the properties of the REPs (e.g., the depolarization ratios of $\rho \approx {}^1/_3$).[16] Moreover, the valence force field analysis of the ν(Cu−Cu) stretching and the δ(Cu−Cu−N_{eq}) bending character of modes ν_1 and ν_2 are consistent with their enhancement, principally in resonance with the $\sigma \rightarrow \sigma^*$ transition. The presence of multiple conformational isomers suggests that there should be a dependence of both the mode frequency of ν_1 and ν_2 and the electronic transition energy. The results of ZINDO/S CI calculations performed as a function of the Cu−Cu bond length are given in Table 3. These results confirm a correlation between the electronic transition energy and the frequency of the Raman-active vibrational modes consistent with experimental results. Lengthening the Cu−Cu bond lowers the transition energy, consistent with the trend observed in the REPs. Experimentally, the peaks of the REPs for isomers 1 and 2 are 13 860 cm^{-1} (ν_1 = 290 cm^{-1}) and 13 190 cm^{-1} (ν_1 = 277 cm^{-1}), respectively. [The REP for isomer 3 appears to have two maxima in ν_1, and the complicated form of the REP seen for ν_2 suggests that vibronic coupling plays a role in the observed REP. Using the value for the ν_2 REP for isomer 3, we have 11 900 cm^{-1}, or using an average value for the ν_1 REP, the peak is found at 12 150 cm^{-1} (ν_1 = 270 cm^{-1}).] On the basis of a bond length/frequency correlation[16] and the correlation of the peak of the REP with the ν_1 frequency for the three isomers, the shift in the absorption band (i.e., peak of the REP in this case) is predicted to be ≈1000 cm^{-1} for a change in bond length of 0.05 Å. Both the bond length/frequency correlations and ZINDO/S CI calculations indicate that the range of bond lengths in Cu_2L is as great as ±0.08 Å in solution. This does not seem unreasonable given the difference of 0.05 Å in the two crystal structures that show isomeric forms of Cu_2L.

Table 3. Calculated Transition Energies and Transition Dipole Moments for the $\sigma \rightarrow \sigma^*$ Absorption Band at 750 nm Based on the ZINDO/S CI Method

Cu−Cu (Å)	$\sigma \rightarrow \sigma^*$ (cm^{-1})	$\sigma \rightarrow \sigma^*$ (D)
2.36	30 326.3	6.62
2.4	29 335.5	6.70
2.45	28 013.3	6.80
2.5	26 780.2	6.91
2.55	25 539.4	7.0

The absorption and Raman spectroscopy of both $Cu_2L(NO_3)_3$ and $Cu_2L(CH_3CO_2)_3$ indicate the presence of multiple conformational isomers in solution. As a test of this, we obtained the resonance Raman frequency of the ν_1 band of both salts as crystalline solids. The two isomers of the Cu_2L structure in the two salts $Cu_2L(NO_3)_3$ and $Cu_2L(CH_3CO_2)_3$ may be related to the isomeric forms in solution. The Raman frequencies of the two crystalline forms are single-component Raman bands of $Cu_2L(NO_3)_3$ $\nu_1 \approx 290$ cm^{-1} and $Cu_2L(CH_3CO_2)_3$ $\nu_1 \approx 287$ cm^{-1} when excited at a sufficiently low laser excitation intensity. In the process of investigating the resonance Raman spectra on polycrystalline samples in a KBr pellet, it was found that the illumination of the acetate salt with laser powers of >100 mW focused onto an ≈30 μm spot size for periods of 20 min resulted in the appearance of a shoulder on the ν_1 band at 276 cm^{-1}. This frequency shift with respect to the pure crystalline band is commensurate with the frequency shifts observed when the crystal is dissolved in an H_2O solution, although it was estimated that only about a 10% conversion of the sample was achieved in 20 min. At low powers (≈15 mW), a single band was observed for both the nitrate and acetate salts.

Discussion

The existence of the isomeric forms of Cu_2L in solution represents an important example of a distortional isomer. In this conformer, the Cu−Cu bond stretch is strongly coupled to N_{eq}−Cu−Cu−N_{eq} torsional deformations. Although bond-stretch

isomerism in a number of inorganic complexes has been discredited on the basis of experimental considerations,[20] there is no theoretical reason to exclude this class of isomerism.[21] The bond-stretch isomerism described here involves a tradeoff between two types of bonding interaction. Both the hydrogen bonding to counterions by the six equatorial N−H groups of Cu_2L and the strain of the octaaza-cryptand ligand L are coupled to $N_{eq}-Cu-Cu-N_{eq}$ torsional distortions. The Cu−Cu bond is sufficiently weak such that its length is also coupled to the $N_{eq}-Cu-Cu-N_{eq}$ torsional coordinate. There is considerable experimental evidence to support this view of the potential energy surface. Although the multiple-component solution resonance Raman spectra of Cu_2L are correlated with the frequency of the absorption band as indicated by the REPs of the Franck−Condon-active modes ν_1 and ν_2, both the acetate and nitrate salts exist as crystallographically well-defined structures[14] in that each display ν_1 and ν_2 as single-component peaks. The band positions of ν_1 in the crystalline forms differ by $\approx 2-3$ cm^{-1}, with the energies of the nitrate peaks corresponding to the highest-frequency component of the ν_1 band in Figure 2 and the acetate peaks being at a lower frequency. The direction of this shift is consistent with the increase of the Cu−Cu bond length in the acetate salt by 0.05 Å relative to the nitrate salt.[14] The ligands L in the two structures are related by a concerted twist coupled to the $N_{eq}-Cu-Cu-N_{eq}$ dihedral angle, which changes from a nearly perfectly staggered D_{3d} geometry (60°) for $Cu_2L(NO_3)_3 \cdot 6H_2O$ to 50° for $Cu_2L(CH_3CO_2)_3 \cdot 6H_2O$ as the ligand L twists. As a consequence of the coupling of the ligand geometry to the Cu−Cu bond length, the frequency of ν_1 is strongly influenced by changing the hydrogen-bonding environment around the ligand. The complete absence of hydrogen bonding, achieved by dissolving the $B(C_6H_5)_4^-$ (tetraphenylborate) salt of Cu_2L in CH_3CN solution, leads to a Raman spectrum having a single-component ν_1 peak at a frequency of 275 cm^{-1}.[16] On the other hand, the dissolution of the acetate salt of Cu_2L in a CH_3CN solution which permits hydrogen bonding results in two dominant components for ν_1: one at 288 cm^{-1} and one at 276 cm^{-1}. In aqueous solutions, where hydrogen bonding to the ligand is likely dominated by the solvent, identical multicomponent spectra for the acetate and nitrate salts are observed, and these are indeed similar to the spectra observed in CH_3CN for the acetate salt.

The ZINDO/S CI calculations provide orbital assignments that are consistent with d−d transitions that are intervalence transitions of the $Cu^{1.5}-Cu^{1.5}$ system held in place by the cryptand ligand. These calculations support the previously mentioned view particularly in that they show that the different isomers likely have slightly different absorption spectra and Raman frequencies for ν_1 and ν_2 and moreover that these are correlated as the experimental data indicate. We have tacitly assumed that the REP of a particular mode tracks the absorption spectrum for that mode. This is indeed the case for Franck−Condon-active modes (A_{1g} modes) in the limit of weak electron−nuclear coupling as is the case here. The apparent breadth of the absorption bands is due to the presence of multiple conformations and rapid electronic dephasing of electronic transitions with d−d character. There is no evidence for the structure that would indicate strong electron−nuclear coupling.

The electroabsorption data indicate that the counterion environment in aqueous solution plays an important role in the determination of the electronic properties of Cu_2L. By symmetry, the dipole moment is zero in all of the states for a molecule of D_3 or D_{3d} symmetry. However, environmental or vibronic symmetry breaking can lead to a significant dipole and, therefore, a significant $\Delta\mu_A$, even in molecules whose idealized point group cannot support a dipole. There is no evidence to indicate strong vibronic coupling because the enhanced Raman modes for the $\sigma \rightarrow \sigma^*$ transition are all Franck−Condon-active modes of A_{1g} symmetry.

Environmental symmetry breaking can arise because of the instantaneous position of the counterions in solution or the frozen configuration of counterions in a glycerol/buffer glass. In the crystal structure of the acetate salt, the acetate counterions are hydrogen bonded to the equatorial N−H groups of the octaaza-crytpand ligand. The conformation of the counterions in solution is not known but can be modeled by placement of counterions around the molecule at various distances from the N−H hydrogen bond sites (see the Supporting Information). ZINDO/S CI calculation systems where the counterion conformation is varied lead to induced equatorial dipole moments, although the axial (*z* polarized) polarizability is larger. The reason for this is that the polarizability in the *xy* plane is roughly half as large as that along *z*, yet the electric field in *xy* is much greater than that along *z* because the counterions hydrogen bond to N−H sites in this plane. This prediction agrees with experiment. By symmetry, the transition moment for $\sigma \rightarrow \sigma^*$ transition is aligned along the Cu−Cu bond while those for the $\delta \rightarrow \sigma^*$ and $\delta^* \rightarrow \sigma^*$ transitions are perpendicular to the Cu−Cu bond. The angles ζ_A give the projection of $\Delta\mu_A$ along the transition dipole moment. The angles ζ_A in Table 2 suggest that the equatorial effect of the counterions dominates, giving rise to a large angle between the $\sigma \rightarrow \sigma^*$ transition and $\Delta\mu_A$.

The sign of $\Delta\alpha$ is negative, indicating that the ground-state polarizability is larger than the excited-state polarizability. Surprisingly, this unusual electronic structure is predicted by the ZINDO/S CI calculations. The fact that the transitions occur from σ and δ levels to a single occupied σ^* level provides a simple explanation. The energy level spacing among these d levels is relatively small compared to the energy-level gap to the next highest level. Using simple models of the polarizability, we show that, under these circumstances, the ground-state polarizability can be larger than the excited-state polarizability.[22,23]

The polarizability change of a two-level system shown in Scheme 1 can be modeled using the Kramers−Heisenberg−Dirac formalism.

Scheme 1

E_1 ——— $|1\rangle$

E_0 ——— $|0\rangle$

The ground-state polarizability is given by

$$\alpha_g = \frac{1}{\hbar}\frac{\langle 0|\mathbf{er}|1\rangle\langle 1|\mathbf{er}|0\rangle}{E_1 - E_0}$$

In this expression, the terms are the transition moments for the electronic transition from state 0 to state 1. The polarization is along the direction given by the unit vector **e**. For a two-level system, the excited-state polarizability is the negative of the

(20) Parkin, G. *Chem. Rev.* **1993**, *93*, 887−911.
(21) Exstrom, C. L.; Britton, D.; Mann, K. R.; Hill, M. G.; Miskowski, V. M.; Schaefer, W. P.; Gray, H. B.; Lamanna, W. M. *Inorg. Chem.* **1996**, *35*, 549−550.
(22) Brunschwig, B. S.; Creutz, C.; Sutin, N. *Coord. Chem. Rev.* **1998**, *177*, 61−79.
(23) Reimers, J. R.; Hush, N. S. *Coord. Chem. Rev.* **1998**, *177*, 37−60.
(24) Liptay, W. *Ber. Bunsen.-Ges.* **1976**, *80*, 207−217.

ground-state polarizability.

$$\alpha_e = \frac{1}{\hbar}\frac{\langle 1|er|0\rangle\langle 0|er|1\rangle}{E_0 - E_1} = -\alpha_g$$

Thus, the difference polarizability is negative.

$$\Delta\alpha = \alpha_e - \alpha_g = -2\alpha_g$$

This is, of course, an artifact of the simplified two-state system used here. However, consideration of the aforementioned argument demonstrates that there will always be a contribution to the polarizability that is negative because of the transition moment for any system. Usually, for a multistate system, this negative difference dipole moment change is outweighed by the positive change from the many higher states. However, for the $\sigma \rightarrow \sigma^*$ and $\delta,\delta^* \rightarrow \sigma^*$ transitions of Cu_2L, it is possible that the relatively large transition moment for an electronic transition that is basically a d−d transition could give rise to a dominant contribution. The s and p states may be significantly higher, and thus, their contribution to the polarizability would be less. To illustrate this, we can consider a three-state system in which the two lowest are much closer in energy than the third. For this system, the polarizability in the ground state is

Scheme 2

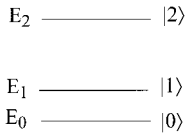

$$\alpha_g = \frac{1}{\hbar}\frac{\langle 0|er|1\rangle\langle 1|er|0\rangle}{E_1 - E_0} + \frac{1}{\hbar}\frac{\langle 0|er|2\rangle\langle 2|er|0\rangle}{E_2 - E_0}$$

and the excited-state polarizability is

$$\alpha_e = \frac{1}{\hbar}\frac{\langle 1|er|0\rangle\langle 0|er|1\rangle}{E_0 - E_1} + \frac{1}{\hbar}\frac{\langle 1|er|2\rangle\langle 2|er|1\rangle}{E_2 - E_1}$$

Thus, the difference polarizability is

$$\Delta\alpha = \alpha_e - \alpha_g = \frac{1}{\hbar}\frac{\langle 1|er|2\rangle\langle 2|er|1\rangle}{E_2 - E_1} - \frac{1}{\hbar}\frac{\langle 0|er|2\rangle\langle 2|er|0\rangle}{E_2 - E_0} - \frac{2}{\hbar}\frac{\langle 1|er|0\rangle\langle 0|er|1\rangle}{E_0 - E_1}$$

The difference polarizability will be negative if the transition moment for the $0 \rightarrow 1$ transition is significantly larger than that for the $1 \rightarrow 2$ transition and particularly if the energy difference $E_1 - E_0 \ll E_2 - E_1$, as indicated in Scheme 2. This model can explain the negative polarizability change observed in Cu_2L. If the transition moments $\sigma \rightarrow \sigma^*$ and $\delta,\delta^* \rightarrow \sigma^*$ are sufficiently large as compared to $\sigma^* \rightarrow$ 4s $\sigma^* \rightarrow$ 4p, the difference polarizability will be negative. Although this simplified three-state description is, at best, only qualitative (possible transition dipole coupling between the three low-lying orbital configurations has not been considered), the general model has also been substantiated by semiempirical ZINDO/S CI calculations, where $\Delta\alpha \approx -68$ Å^3 is found to be an upper bound to the difference polarizability for the $\sigma \rightarrow \sigma^*$ (Supporting Information). The fact that the polarizability is greater along the Cu−Cu bond is consistent with the larger experimental values of $\Delta\alpha$ and Tr($\Delta\alpha$) for the $\sigma \rightarrow \sigma^*$ transition as compared with the $\delta,\delta^* \rightarrow \sigma^*$ transitions (Table 2). These values indicate that the dominant term in the difference polarizability is $\Delta\alpha_{zz} > \Delta\alpha_{xx} = \Delta\alpha_{yy}$, consistent with the experimental parameters found in Table 2. The transition moment of the $\sigma \rightarrow \sigma^*$ transition is along the z axis, and thus, the projection of Tr($\Delta\alpha$) on $\Delta\alpha$ is larger for this electronic transition than for the $\delta,\delta^* \rightarrow \sigma^*$ transitions.

Conclusion

The study presented here provides new insights into the interpretation of electroabsorption spectroscopy in inorganic complexes. We have shown, using a simple model, that the difference polarizability can be expected to be negative for transitions among d states that are well-separated from other higher-lying s and p states. The procedure for estimating the difference polarizability given here can be applied generally to systems where there are a limited number of energetically accessible states. The electroabsorption data suggest that symmetry breaking due to the counterions induces a dipole moment. The first observation of this type of symmetry breaking was seen in $Ru(bipy)_3$, where the D_3 symmetry of the molecule must be broken to give rise to the large value of $\Delta\mu_A$ observed in the MLCT transition. The data and analysis provided here indicate that this phenomenon may be applied generally to inorganic complexes.

The weakness of the Cu−Cu bond gives rise to substantial conformational flexibility in dimeric copper complexes. Electroabsorption and Raman data present a detailed view of the electronic structure and the potential energy surface of one such complex, Cu_2L. A structural picture emerges based on the comparison of these data to the X-ray crystal data on the acetate and nitrate salts of Cu_2L. The torsional coordinate N_{eq}−Cu−Cu−N_{eq} is strongly coupled to the Cu−Cu bond stretch. The torsional coordinate is affected both by the ligand geometry and the hydrogen-bonding environment. The coupling of a torsional coordinate to a bond stretch provides an example of bond-stretch isomerism. Although the original claim for bond-stretch isomerism was flawed by unrecognized disorder problems,[20] bond-stretch isomerism coupled to ligand deformation or distortional isomerism is recognized as a viable mechanism for multiple minima.[21] Evidence for such isomers coexisting as true minima in solution has been lacking. The present data present further evidence for the coexistence of such isomers in solution.

The complex studied here mimics the dimeric copper complex in the Cu_A site of cytochrome *c* oxidase and nitrite reductase in several important respects. Both have stable mixed-valent forms. Both have three visible and near-infrared absorption bands that originate from d−d transitions of coupled metal centers. Both have low-frequency Raman bands that are consistent with a Cu−Cu bond. However, the copper dimer in Cu_2L provides an example of the importance of isomerism in Cu−Cu bonded systems that is not immediately apparent in the Raman and absorption spectra of the Cu_A site. Regarded as a model system, the Cu−Cu bond of Cu_2L indicates the importance of considering multiple isomers that may not be immediately apparent in the resting state of an enzyme. In cytochrome oxidase, the possibility of such control by subtle changes in the ligand environment could be critically important in the function of the Cu_A subunit, which serves to shuttle electrons to the enzyme's catalytic site. Both the large Debye−Waller terms found by EXAFS for the binuclear Cu_A center of cytochrome oxidase[8,9] and strong mixing of metal and sulfur orbitals[6,10] may be related to the control of electron transfer in the enzyme.

Acknowledgment. S.F. was supported by a Los Alamos Director's Fellowship. S.G.B. was supported in part by the NSF Chemistry Program. The authors thank Dr. M. H. Whangbo of NCSU for helpful discussions.

Supporting Information Available: Figures showing fitting of the absorption spectra at 295 and 77 K, fitting of the resonance Raman spectra at 295 and 40 K, and relevant molecular orbitals. Output from semiempirical calculations are cited in the text. The details of the normal-mode analysis and additional isotopic substitution data are presented. This material is available free of charge via the Internet at http://pubs.acs.org.

IC010494G